Cascaded Downscaling–Calibration Networks for Satellite Precipitation Estimation

Yinghong Jing, Liupeng Lin, Xinghua Li, *Senior Member, IEEE*, Tongwen Li, *Member, IEEE*, and Huanfeng Shen, *Senior Member, IEEE*

***Abstract*— Precipitation is a critical process in the terrestrial hydrological circulation, affecting climate change, water resource management, and agricultural production. Satellite-borne observations have prominent advantages in macro and mesoscopic quantitative precipitation estimation. Nevertheless, they are subject to low spatial resolution and inherent biases. Therefore, this study utilizes the surface–surface downscaling network and point–surface fusion network for fine-resolution and high-precision precipitation mapping over China. To deeply explore the complicated relationships between various ancillary factors, ground measurements, and satellite precipitation, an attention mechanism-based convolutional network (AMCN) is used for spatial downscaling and a geo-intelligent deep belief network (Geoi-DBN) is used for ground–satellite fusion. Experimental results indicate that cascaded networks toward two different objectives are superior to baseline methods, achieving R^2 and root mean square error (RMSE) of about 0.84 and 27.23 mm/month, respectively. Besides, the assistance of geo-intelligent items and ancillary factors contributes to fusion accuracy. This study provides an effective way for precipitation estimation over China.**

***Index Terms*— Convolutional network, deep belief network, ground–satellite fusion, precipitation, spatial downscaling.**

I. Introduction

PRECIPITATION is a typical hydrometeorological parameter associated with hydrological circulation, climate change, and socioeconomic development [1]. Ground measurements can accurately reflect the distribution characteristics of precipitation at the point scale. Nevertheless, their applications are severely limited by meteorological stations with the uneven and sparse distribution. Therefore, satellite observations are extensively used for global and regional quantitative precipitation estimation. However, satellite precipitation products are generally difficult to be used for refined investigations due to their low spatial resolution and nonnegligible biases [2]. Therefore, enhancing satellite precipitation with spatial downscaling and ground–satellite fusion is of great significance for related hydrological and meteorological researches.

Numerous algorithms were developed to downscale satellite precipitation data, such as multiple linear regression [3], random forest [4], Cubist [5], and convolutional neural network [6]. In addition, various bias adjustment methods were proposed to calibrate satellite precipitation data with ground measurements, such as geographical difference analysis (GDA) [7], geographically weighted regression [8], and spatiotemporal disaggregation calibration algorithm [9]. For the downscaling–calibration procedure, Ezzine et al. [10] introduced the stepwise regression and GDA. Chen et al. [11] utilized the same spatial random forest approach to downscale and calibrate satellite precipitation. However, these studies generally emphasized a single task, such as spatial downscaling or ground–satellite fusion. The final results were still subject to low spatial resolution or inconsistent regional accuracy.

Consequently, considering the data characteristics of spatial downscaling and ground–satellite fusion, this study combines the attention mechanism-based convolutional network (AMCN) and geo-intelligent deep belief network (Geoi-DBN) to estimate fine-resolution and high-precision precipitation over China. Cascaded networks can fully exploit the latent associations between precipitation and ancillary factors and the geographical autocorrelation of ground measurements.

The remainder of this letter is arranged as follows. The method is introduced in Section II. The experiments are described in Section III, followed by conclusion in Section IV.

II. Proposed Methodology

A. Overall Framework

AMCN and Geoi-DBN are cascaded to downscale and calibrate satellite precipitation, as shown in Fig. 1.

First, high-resolution precipitation data are estimated from low-resolution satellite observations, which is a surface-to-surface process. Convolutional neural networks capable of efficiently extracting spatial information from high-dimensional data are considered applicable to spatial downscaling. Therefore, an AMCN proposed in our last research is used for satellite precipitation downscaling, which models the relationship between precipitation and input data including low-resolution precipitation and high-resolution ancillary data [6]. Specifically, AMCN-based downscaling can be formulated as

$$X = f_u(Y) + \xi(Y, F_A) \tag{1}$$

Manuscript received 24 September 2022; accepted 10 October 2022. Date of publication 12 October 2022; date of current version 27 October 2022. This work was supported in part by the National Key Research and Development Program of China under Grant 2019YFB2102900 and in part by the Open Fund of Hubei Luojia Laboratory under Grant 220100055. *(Yinghong Jing and Liupeng Lin are co-first authors.) (Corresponding author: Xinghua Li.)*

Yinghong Jing, Liupeng Lin, and Huanfeng Shen are with the School of Resource and Environmental Sciences, Wuhan University, Wuhan 430079, China (e-mail: yhjing@whu.edu.cn; linliupeng@whu.edu.cn; shenhf@whu.edu.cn).

Xinghua Li is with the School of Remote Sensing and Information Engineering, Wuhan University, Wuhan 430079, China (e-mail: lixinghua5540@whu.edu.cn).

Tongwen Li is with the School of Geospatial Engineering and Science, Sun Yat-sen University, Zhuhai 519082, China (e-mail: litw8@mail.sysu.edu.cn).

Digital Object Identifier 10.1109/LGRS.2022.3214083

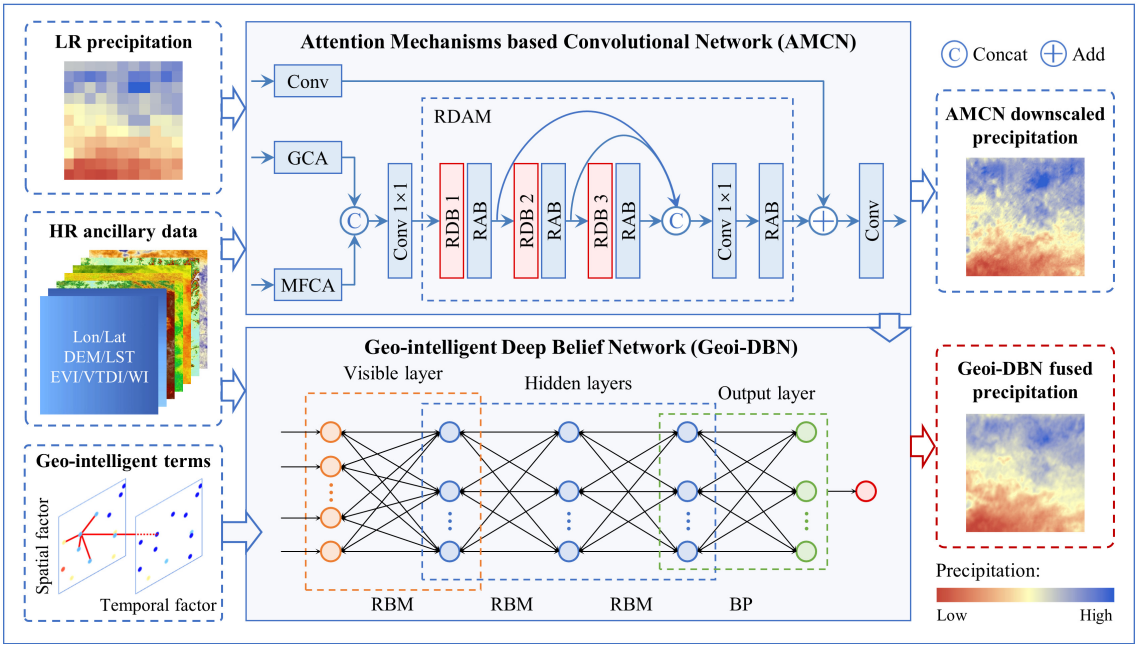

Fig. 1. Proposed downscaling–calibration procedure. Note that LR and HR denote low resolution and high resolution, respectively.

where Y and X represent the low-resolution and high-resolution precipitation, respectively. F_A represents the various ancillary factors, which contain longitude, latitude, elevation, enhanced vegetation index, daytime/nighttime surface temperature, temperature-vegetation dryness index, normalized difference water index (NDWI), and land surface water index (LSWI). In addition, $f_u(\cdot)$ is the bilinear upsampling function. $\xi(\cdot)$ denotes the residual convolutional network.

Subsequently, ground measurements are incorporated into downscaled satellite precipitation data by a Geoi-DBN method. Geoi-DBN proposed by [12] is an advanced point–surface fusion method. It has been successfully applied to the inversion of multiple meteorological parameters, such as $PM_{2.5}$ and temperature. It is introduced and modified to fuse ground and satellite precipitation, which can be expressed as

$$P_F = f(P_R, F_A, P_{G-S}, P_{G-T}, D, T) \tag{2}$$

where P_F and P_R indicate the fused precipitation and downscaled remote-sensed precipitation (i.e., X), respectively. $T = \{1, 2, \ldots, \text{total time}\}$ is a time parameter measuring temporal heterogeneity. Moreover, three geo-intelligent items are introduced to capture the geographical autocorrelation of ground precipitation. P_{G-S} and P_{G-T} represent the spatially and temporally autocorrelated precipitation factors, respectively. D represents a distance parameter reflecting the uneven distribution of meteorological stations.

The fine-resolution and high-precision precipitation data can be generated through cascaded networks. AMCN and Geoi-DBN are detailed in subsequent sections.

B. AMCN

AMCN consists of a global cross-attention (GCA) module, a multifactor cross-attention (MFCA) module, and a residual densely connected module embedded with an attention mechanism (RDAM).

GCA and MFCA are two cross-attention modules to enhance complementary information from low-resolution precipitation and high-resolution ancillary factors. In GCA, the integrated ancillary factors provide detailed information and low-resolution precipitation provides distribution information. Moreover, considering the significant differences among ancillary factors, MFCA consisting of multiple cross-attention blocks for each ancillary factor and low-resolution precipitation is used to enhance feature extraction.

Subsequently, an RDAM consisting of a densely connected three-layer structure is used to extract deep features. Each layer contains a residual dense block (RDB) and a residual attention block (RAB). RDAM can simultaneously extract and recalibrate deep characteristics of low-resolution precipitation and high-resolution ancillary factors. Then, the fine-resolution satellite precipitation can be obtained through global residual learning. Last but not least, the Charbonnier loss and degradation loss are combined to constrain the network training. The converged network is then utilized for testing. More details on spatial downscaling can refer to our previous work [6].

C. Geoi-DBN

DBN is a typical deep learning model with the restricted Boltzmann machine (RBM) as a basic unit [13]. The network is composed of multiple RBMs and a back-propagation (BP) layer. Each RBM consists of a visible layer and a hidden layer. In this study, three RBMs, each with 15 neurons, are cascaded for feature extraction, and then, a BP layer is used for precipitation estimation.

In addition, as a typical hydrometeorological parameter, precipitation is strongly autocorrelated in time and space. Therefore, three geo-intelligent items are designed in Geoi-DBN to fully capture the geographical autocorrelation. They are calculated as follows:

$$P_{G-S} = \frac{\sum_{i=1}^{n} w_{s,i} \times P_{s,i}}{\sum_{i=1}^{n} w_{s,i}}, \quad w_{s,i} = \frac{1}{d_{s,i}^2} \tag{3}$$

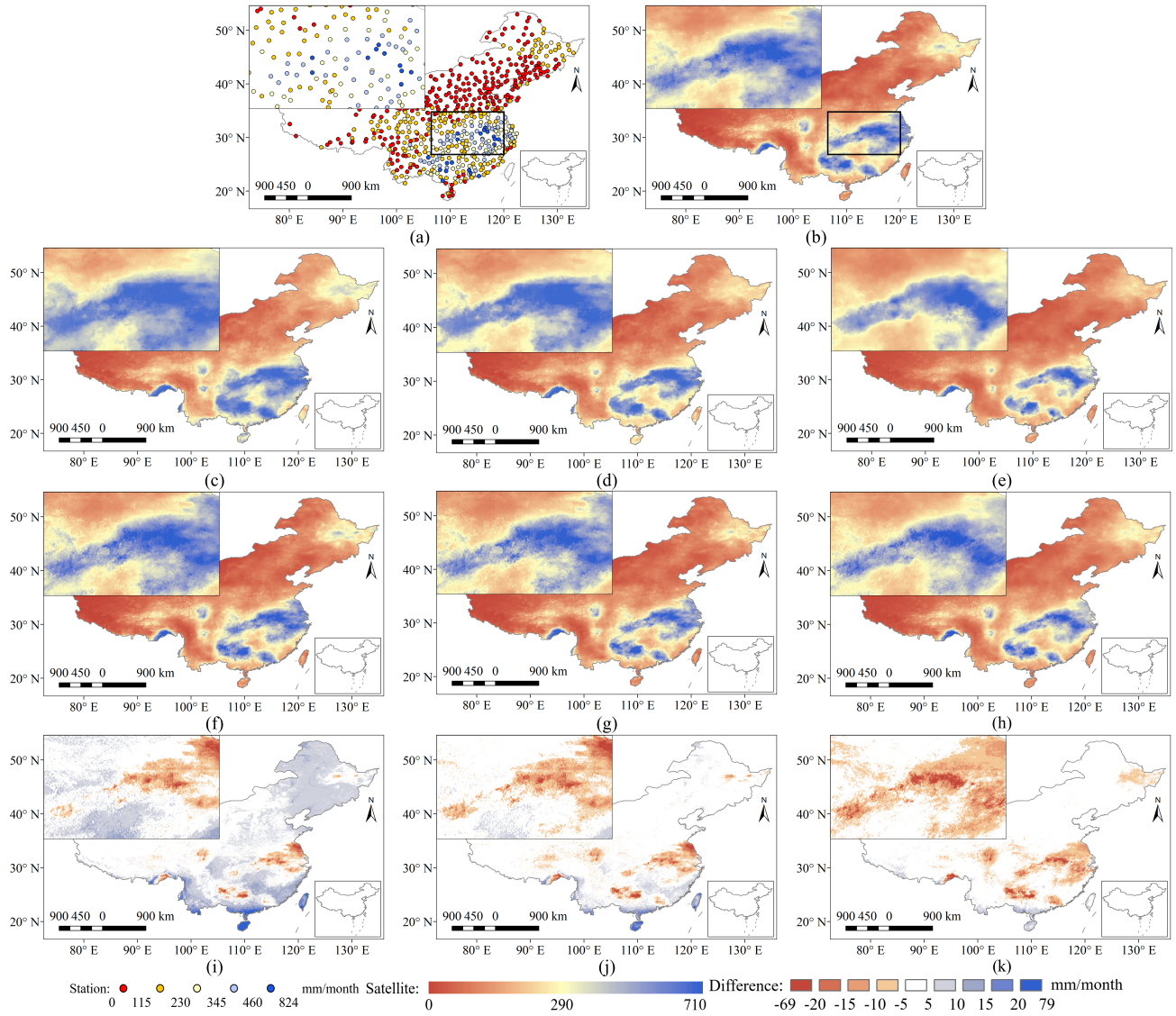

Fig. 2. Downscaled results of RF and AMCN and the calibrated results of GDA and Geoi-DBN for two downscaled groups in June 2020. (a) Ground measurements. (b) Original GPM IMERG precipitation. (c) RF downscaled precipitation. (d) RF downscaled and GDA calibrated data. (e) RF downscaled and Geoi-DBN calibrated data. (f) AMCN downscaled precipitation. (g) AMCN downscaled and GDA calibrated data. (h) AMCN downscaled and Geoi-DBN calibrated data. (i) Difference after RF and AMCN. (j) Difference after RF–GDA and AMCN–GDA. (k) Difference after RF–Geoi-DBN and AMCN–Geoi-DBN.

$$P_{G-T} = \frac{\sum_{j=1}^{m} w_{t,j} \times P_{t,j}}{\sum_{j=1}^{m} w_{t,j}}, \quad w_{t,j} = \frac{1}{d_{t,j}^2} \tag{4}$$

$$D = \frac{1}{\min(d_{s,i})}, \quad i = 1, 2, \ldots, n \tag{5}$$

where $P_{s,i}$ and $P_{t,j}$ are the precipitation of the ith station in the spatial neighborhood and the jth prior reference in the temporal neighborhood, respectively. w_s and w_t are the spatial and temporal weights, respectively. d_s and d_t denote the spatial and temporal distances, respectively. n and m denote the numbers of spatially adjacent stations and temporally adjacent grids, respectively, which are set to 10 and 1 in this study. The combination of these factors can fully express the geographical autocorrelation of precipitation.

III. Experiments

To evaluate the effectiveness of cascaded networks, monthly precipitation datasets from Integrated Multi-satellitE Retrievals for Global Precipitation Mission (GPM Integrated Multi-satellitE Retrievals for the GPM mission (IMERG) [14]) and ground measurements from 605 meteorological stations over China were used as the primary study data. Multiple ancillary factors were derived from moderate resolution imaging spectroradiometer (MODIS) products and Shuttle Radar Topography Mission (SRTM) digital elevation model (DEM) dataset. It has been reported that IMERG-Final shows the highest performance at the monthly resolution among multiple precipitation products [15]. However, the original IMERG-Final precipitation datasets also have some uncertainties, with an average bias of 14.43 mm/month for the study data (see Table I). Therefore, the following experiments were designed to improve the resolution and accuracy of the original datasets. Specifically, RF and GDA were introduced as the baseline methods of downscaling and calibration, respectively. GDA is a bias adjustment method based on inverse distance weighting.

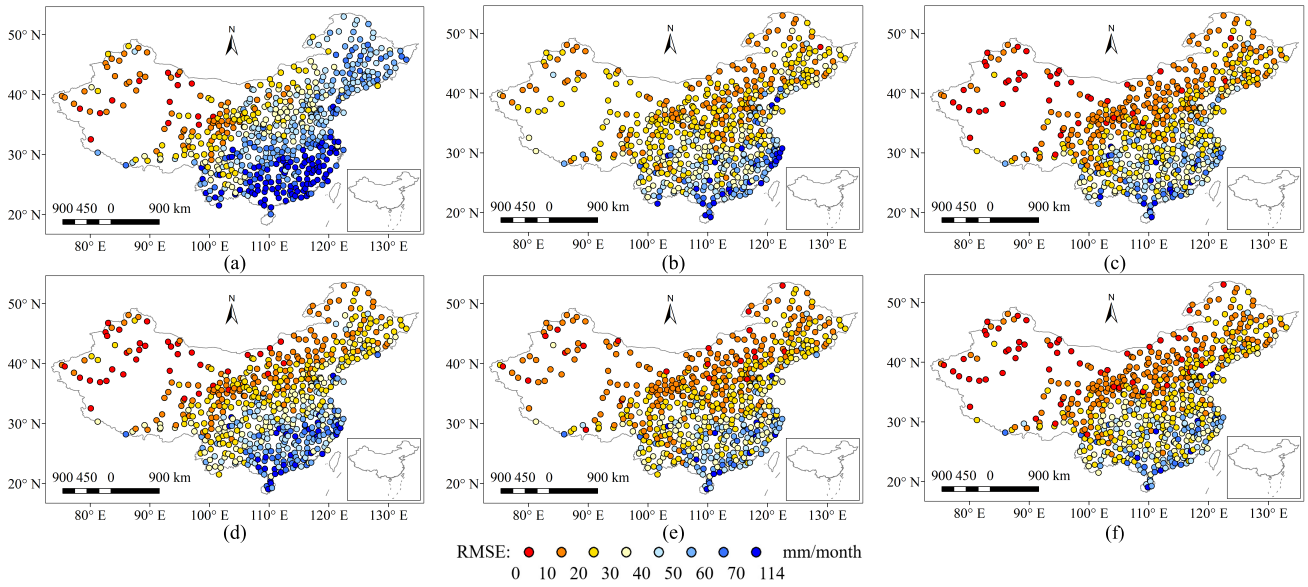

Fig. 3. Spatial patterns of RMSEs of all downscaled and calibrated precipitation data compared with ground measurements. (a) RF downscaled precipitation. (b) RF downscaled and GDA calibrated data. (c) RF downscaled and Geoi-DBN calibrated data. (d) AMCN downscaled precipitation. (e) AMCN downscaled and GDA calibrated data. (f) AMCN downscaled and Geoi-DBN calibrated data.

TABLE I
QUANTITATIVE EVALUATION RESULTS (UNIT: MM/MONTH)

Downscaling	Calibration	R^2	Bias	RMSE
Original	––	0.83	14.43	35.37
RF	––	0.77	35.64	53.16
	GDA	0.78	-0.50	35.13
	Geoi-DBN	0.81	0.74	29.76
AMCN	––	0.83	13.64	34.97
	GDA	0.83	-0.42	29.42
	Geoi-DBN	**0.84**	**0.08**	**27.23**

First, RF and AMCN were used to downscale original satellite precipitation from 0.1° to 0.01°. The models were trained on low-resolution data from January 2018 to December 2018. The inputs contained downsampled satellite precipitation at a 1° resolution and ancillary factors at a 0.1° resolution. The labels were original satellite precipitation at a 0.1° resolution. Then, the models were tested on original satellite precipitation from January 2019 to December 2020, assisted by ancillary data at a 0.01° resolution. Subsequently, GDA and Geoi-DBN were used to calibrate two downscaled precipitation datasets by incorporating ground measurements. Finally, precipitation datasets with fine resolution and high precision over China can be generated. This section presents the cross-comparison experiment and the ablation experiment.

A. Cross-Comparison Experiment

In terms of visual effects, the downscaled and calibrated results in June 2020 are shown in Fig. 2. Compared with ground measurements, the original GPM IMERG precipitation data expand areas with high precipitation. RF downscaled results significantly magnify this phenomenon, while AMCN downscaled results superiorly preserve the original accuracy. The spatial patterns of precipitation differences between these datasets (rows 2 and 3) are shown in row 4. The difference map reveals that RF significantly underestimates high precipitation and overestimates low precipitation. Then, based on two downscaled results, the effectiveness of Geoi-DBN for bias adjustment by ground–satellite fusion is compared with GDA. Both methods can prominently calibrate the overestimation amplified by RF, especially in Northeast China. However, GDA is difficult to improve regions with mixed positive and negative biases because it only exploits spatial similarity and ignores spatial variability. By contrast, Geoi-DBN ameliorates more overestimated regions, especially in Southeast China.

For in-depth assessment, the experimental results are quantitatively evaluated by a tenfold cross-validation strategy, as shown in Table I. AMCN is prominently superior to RF in satellite precipitation downscaling, with R^2 increased by 0.06 and the root mean square error (RMSE) decreased by 18.19 mm/month. It can effectively extract details from various ancillary factors, attributing to its feature richness. Subsequently, the inherent biases of satellite precipitation data are significantly decreased by incorporating ground measurements. GDA can remove biases straightforwardly, thus widely used in satellite precipitation researches. However, it has considerable uncertainty due to its weak consideration of spatial variability. Therefore, this method is not recommended in areas with complex precipitation patterns and sparsely distributed stations. Geoi-DBN obtains superior quantitative evaluation metrics. On the one hand, it fully reflects the spatial variability of biases by using ancillary factors. On the other hand, it further enhances the effectiveness of calibration by considering the geographical autocorrelation of ground precipitation. Compared with RF and AMCN downscaled precipitation datasets, the corresponding calibrated results are significantly improved, with RMSEs decreased by 23.40 and 7.74 mm/month, respectively. For the downscaling–calibration procedure, AMCN–Geoi-DBN obtains optimal accuracy, with R^2 and RMSE of about 0.84 and 27.23 mm/month, respectively.

Moreover, the spatial RMSEs between these precipitation datasets and gauge observations are shown in Fig. 3. RF downscaled results have high RMSEs in the northeastern and

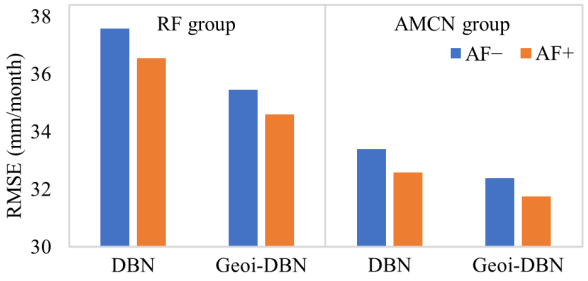

Fig. 4. Calibrated results of DBN and Geoi-DBN with ancillary factors (AF+) and without ancillary factors (AF−), based on RF and AMCN downscaled precipitation data.

southern regions. By contrast, the spatial RMSEs of AMCN are generally lower than those of RF throughout the study area. GDA significantly improves most of the overestimates but overcalibrates some low-precipitation regions, such as northwest China. However, Geoi-DBN obtains a balanced calibration effect, since it extracts sufficient spatial variability from ancillary factors and achieves optimal fusion with few artifacts through the constraints of geo-intelligent items.

Overall, the advantage of cascaded networks is that specialized network structures can be designed for different objectives to make full use of effective information from different data sources.

B. Ablation Experiment

A comparative experiment of DBN and Geoi-DBN with and without ancillary factors is performed to further discuss the importance of geo-intelligent items and ancillary factors in the calibration process, as shown in Fig. 4. Both RF and AMCN groups show that the assistance of geo-intelligent items and ancillary factors contributes to improve the calibrated results. On the one hand, Geoi-DBN obtains lower RMSEs than DBN, since it considers the geographical autocorrelation of ground precipitation by using geo-intelligent items. On the other hand, Geoi-DBN with ancillary factors further decreases RMSEs. There are two reasons for this phenomenon. First, various ancillary factors from MODIS are correlated with precipitation, and DBN can capture their potential associations to improve the fusion. Second, since satellite precipitation downscaling partially relies on ancillary factors, the calibration takes them as inputs, considering the uncertainties of downscaling. However, ancillary factors should be carefully screened and preprocessed, as low-quality factors are likely to introduce additional noise. In this study, multiple tests show that the combination of nine ancillary factors obtains optimal results. Among them, the two water indices (NDWI and LSWI) have the least importance.

IV. Conclusion

In this study, a new downscaling–calibration procedure, AMCN–Geoi-DBN, is designed for fine-resolution and high-precision precipitation estimation, which combines the advantages of the surface–surface downscaling network and point–surface fusion network. Compared with RF, AMCN can effectively incorporate ancillary factors through deep feature extraction and thus obtain downscaled satellite precipitation data with higher accuracy. In addition, Geoi-DBN can comprehensively consider the geographical autocorrelation in ground measurements and spatial variability in ancillary factors. Experiments reveal that AMCN–Geoi-DBN significantly improves the accuracy of spatial downscaling and ground–satellite fusion compared to all baseline methods. Consequently, it is promising for refined and accurate precipitation estimation. Furthermore, an improved downscaling–calibration procedure for satellite precipitation with a higher temporal resolution is a future direction.

References

[1] T. Lincoln, "Climate science: A bright side of precipitation," *Nature*, vol. 455, no. 7211, p. 298, 2008.

[2] X. Su, C. K. Shum, and Z. Luo, "Evaluating IMERG V04 final run for monitoring three heavy rain events over mainland China in 2016," *IEEE Geosci. Remote Sens. Lett.*, vol. 15, no. 3, pp. 444–448, Mar. 2018.

[3] S. Jia, W. Zhu, A. Lũ, and T. Yan, "A statistical spatial downscaling algorithm of TRMM precipitation based on NDVI and DEM in the Qaidam basin of China," *Remote Sens. Environ.*, vol. 115, pp. 3069–3079, Dec. 2011.

[4] J. Zhang, H. Fan, D. He, and J. Chen, "Integrating precipitation zoning with random forest regression for the spatial downscaling of satellite-based precipitation: A case study of the Lancang–Mekong river basin," *Int. J. Climatol.*, vol. 39, no. 10, pp. 3947–3961, Aug. 2019.

[5] Z. Ma, Z. Shi, Y. Zhou, J. Xu, W. Yu, and Y. Yang, "A spatial data mining algorithm for downscaling TMPA 3B43 V7 data over the Qinghai–Tibet plateau with the effects of systematic anomalies removed," *Remote Sens. Environ.*, vol. 200, pp. 378–395, Oct. 2017.

[6] Y. Jing, L. Lin, X. Li, T. Li, and H. Shen, "An attention mechanism based convolutional network for satellite precipitation downscaling over China," *J. Hydrol.*, vol. 613, Oct. 2022, Art. no. 128388.

[7] F. I. Boushaki, K.-L. Hsu, S. Sorooshian, G.-H. Park, S. Mahani, and W. Shi, "Bias adjustment of satellite precipitation estimation using ground-based measurement: A case study evaluation over the southwestern United States," *J. Hydrometeorol.*, vol. 10, no. 5, pp. 1231–1242, Oct. 2009.

[8] L. Chao, K. Zhang, Z. Li, Y. Zhu, J. Wang, and Z. Yu, "Geographically weighted regression based methods for merging satellite and gauge precipitation," *J. Hydrol.*, vol. 558, pp. 275–289, Mar. 2018.

[9] Z. Ma et al., "AIMERG: A new Asian precipitation dataset (0.1°/half-hourly, 2000–2015) by calibrating the GPM-era IMERG at a daily scale using APHRODITE," *Earth Syst. Sci. Data*, vol. 12, no. 3, pp. 1525–1544, 2020.

[10] H. Ezzine, A. Bouziane, D. Ouazar, and M. D. Hasnaoui, "Downscaling of TRMM3B43 product through spatial and statistical analysis based on normalized difference water index, elevation, and distance from sea," *IEEE Geosci. Remote Sens. Lett.*, vol. 14, no. 9, pp. 1449–1453, Sep. 2017.

[11] C. Chen, B. Hu, and Y. Li, "Easy-to-use spatial random-forest-based downscaling-calibration method for producing precipitation data with high resolution and high accuracy," *Hydrol. Earth Syst. Sci.*, vol. 25, no. 11, pp. 5667–5682, Nov. 2021.

[12] T. Li, H. Shen, Q. Yuan, X. Zhang, and L. Zhang, "Estimating ground-level $PM_{2.5}$ by fusing satellite and station observations: A geo-intelligent deep learning approach," *Geophys. Res. Lett.*, vol. 44, no. 23, pp. 11985–11993, 2017.

[13] G. E. Hinton, S. Osindero, and Y.-W. Teh, "A fast learning algorithm for deep belief nets," *Neural Comput.*, vol. 18, no. 7, pp. 1527–1554, Aug. 2006.

[14] G. J. Huffman, E. F. Stocker, D. T. Bolvin, E. J. Nelkin, and J. Tan. *GPM Imerg Final Precipitation L3 1 Month 0.1 Degree X 0.1 Degree V06*. [Online]. Available: https://10.5067/GPM/IMERG/3B-MONTH/06

[15] J. Xu, Z. Ma, S. Yan, and J. Peng, "Do ERA5 and ERA5-land precipitation estimates outperform satellite-based precipitation products? A comprehensive comparison between state-of-the-art model-based and satellite-based precipitation products over mainland China," *J. Hydrol.*, vol. 605, Feb. 2022, Art. no. 127353.